Title: 21st Century Changes in Global Small-Size Aerosols from Combustion Emissions

Meemong Lee[1], John R. Worden[1], Rebecca Bucholz[2], Helen Worden[2], Mijeong Park, Yuan Wang[3], Jiani Yang[3], Marcin Witek[1], Hui Su[1], Brendan Byrne[1], Kazu Miyazaki[1], Jonathan H. Jiang[1]

[1]Jet Propulsion Laboratory. California Institute for Technology, Pasadena, CA

[2]National Center for Atmospheric Research, Boulder, CO

[3]Division of Geological and Planetary Sciences, California Institute of Technology, Pasadena, CA

Corresponding author: John Worden (john.r.worden@jpl.nasa.gov)

Key Points:

Observed changes in small particle AOD in fire prone regions are related to CO emissions and not CO concentrations.

Changes in combustion emissions in industrialized countries are correlated with AOD variations.

Surface PM2.5 as inferred from these changes have declined in many parts of the globe.

Plain Language Summary

Aerosols have many different types of sources, e.g. farming, fires, power plants, transportation, dust, and have large impacts on human health and on climate. We quantify combustion emissions using satellite observations of carbon monoxide and show that satellite observations of changes in small particle AOD across the globe are linked to changes in these combustion sources. These data and model updates indicate substantial declines of PM2.5 (aerosols that have strong, deleterious effects on human health) across many parts of the globe from changes in combustion emissions.

Abstract Changes in aerosol optical depth, both positive and negative, are observed across the globe during the 21rst Century. However, attribution of these changes to specific sources is largely uncertain as there are multiple contributing natural and anthropogenic sources that produce aerosols either directly or through secondary chemical reactions. Here we show that satellite-based changes in small-mode AOD between 2002 and 2019 observed in data from MISR can primarily be explained by changes, either directly or indirectly, in combustion emissions. We quantify combustion emissions using MOPITT total column CO observations and the adjoint of the GEOS-Chem global chemistry and transport model. The *a priori* fire emissions are taken from the Global Fire Emission Data base with small fires (GFED4s) but with fixed *a priori* for non-fire emissions. Aerosol precursor and direct emissions are updated by re-scaling them with the monthly ratio of the CO posterior to prior emissions. The correlation between modeled and observed AOD improves from a mean of 0.15 to 0.81 for the four industrial regions considered and from 0.52 to 0.75 for the four wildfire-dominant regions considered. Using these updated emissions in the GEOS-Chem global chemistry transport model, our results indicate that surface PM2.5 have declined across many regions of the globe during the 21^{rst} century. For example, PM2.5 over China has declined by ~30% with smaller fractional declines in E. USA and Europe (from fossil emissions) and in S. America (from fires). These results highlight the importance of forest management and cleaner combustion sources in improving air-quality.

1. Introduction

Aerosols have substantive but contrasting impacts on air-quality and climate. Aerosols can impose either positive or negative changes in radiative forcing directly by scattering or absorbing sunlight type (e.g., Satheesh and Ramanathan 2000) or indirectly by changing cloud and rainfall characteristics (e.g. Andrae *et al*. 2004; Andrae and Rosenfeld 2008; Rosenfeld *et al*. 2014; Jiang *et al*. 2018). These different effects depend on the aerosol type as well as its source. For example, fires can emit both scattering and absorbing aerosols with a range of sizes leading to potentially positive or negative impacts on radiative forcing and rainfall (e.g. Kaufmann *et al*. 2005; Koren *et al*. 2012; Sato *et al*. 2018). Despite these wide-ranging effects of aerosols on climate it is thought that the direct and indirect effects of aerosols have a net cooling impact on climate, albeit with uncertainties that are as large as the corresponding radiative forcing

estimates, suggesting their net impact is still not well understood (e.g. Seinfeld *et al*. 2016; Fan *et al*. 2016 and refs therein). While this net cooling effect potentially mitigates some of the climate impact from rising greenhouse gases, an increase in surface aerosols generally leads to poor health outcomes (e.g. Cohen *et al*. 2015 and refs therein). Understanding the location of aerosol emissions and their types is therefore critical towards understanding global climate and health outcomes as a consequence of anthropogenic activities and changes.

Previous studies using satellite and ground-based data have shown significant changes in the aerosol burden during the 21rst century in many industrialized regions (e.g., Donkelaar *et al*. 2015; Mheta *et al*. 2016; Zhao *et al*. 2017). For example, the eastern USA and western Europe show declines in aerosol loading whereas China shows a strong increase in the early 21rst century followed by a decrease in the second decade (Wang *et al*. 2015). In contrast, India shows a steady increase in aerosol loading (Dey and Girolamo 2011; Zhao *et al*. 2017). While the causes of these changes are likely related to human activities the exact attribution is uncertain as agriculture, construction, biomass burning, the automobile and energy sector all contribute significantly to dust and aerosols either directly or indirectly through emission of aerosol pre-cursors and subsequent chemical transformation. Natural sources of aerosols such as biogenic secondary organic aerosols, sea salt, and mineral dust also contribute substantively to the overall aerosol burden (e.g. Jaegle *et al*. 2011; Mahowald 2011; Rosenfeld *et al*. 2014; Bauer *et al*. 2019). In this manuscript we focus on attribution of small-mode aerosols as measured by the Multi-angle Imaging Spectroradiometer (MISR) (e.g., Ragray *et al*. 2010 and refs therein) as these are primarily associated with aerosols from combustion sources and contribute significantly to surface PM2.5 (e.g. Eck *et al*. 2010). Figure 1 (top left) shows the total AOD for small-mode particles from the MISR instrument. As seen in Figure 1, Central Africa is one of the largest sources of small-mode aerosols and is likely related to biomass burning and dust (e.g., Roberts *et al*. 2001). Direct emission from combustion sources, as well as secondary aerosol formation from ammonia and sulfates are the largest sources of aerosols in East Asia (e.g., Huang *et al*. 2014). Over India (e.g. Ramanathan *et al*. 2001; 2005) large sources of aerosols are related to agriculture, transport, coal plants, biomass and biofuel burning, and construction. Similarly, direct and secondary aerosol sources in the USA are likely related to energy, transportation, and agricultural sectors (e.g., Liao *et al*. 2007; Burney 2020).

Observed changes in the small-mode AOD (from MISR) are shown in the bottom left panel of Figure 1. These changes are consistent with observations of aerosols using multiple satellite and ground measurements in the industrial regions of North America, Europe, India, and Asia with the largest changes

in India and Asia but also in South America and smaller but observable changes in the Eastern USA Western Europe, Africa and Australia (e.g. Bucholz *et al.* 2020). These regions have also seen substantive changes in combustion emissions and aerosol pre-cursors as found by satellite observations of trace gasses such as CO, NH_3, SO_2, and NO_2 (e.g., Jiang *et al*. 2015; Yin *et al*. 2015; Warner *et al*. 2015; Hilboll *et al*. 2013; Krotkov *et al*. 2016; Jiang *et al*. 2017). Recently, Buchholz *et al*. (2021) examined multi-decadal trends in both AOD and CO abundance from the NASA Terra Moderate resolution Imaging Spectrometer (MODIS) and Measurements of Pollution in the Troposphere (MOPITT) satellite instruments respectively and found significant spatial and temporal correlations in regions with high biomass burning activity, suggesting a causal link between CO (a tracer for combustion) and AOD. However, CO and aerosols have different photochemical lifetimes leading to seasonal cycles in abundance that are often out of phase in industrial regions, which complicate the attribution of the relationship between these atmospheric species. Therefore, in this research we quantify global CO emissions using almost two decades of satellite observations integrated into a global chemistry transport model to determine to what extent decadal changes in combustion emissions can explain changes in small-mode aerosols and corresponding optical depth.

2. Change in Combustion Emissions and Corresponding Small-mode AOD

Atmospheric carbon monoxide (CO) is a product of the oxidation of atmospheric hydrocarbons and non-methane volatile organic carbons and is also emitted during burning of fossil fuels as a result of incomplete combustion. CO emissions have been quantified from a variety of aircraft and satellite data using global and regional chemistry transport models and different inversion approaches for relating observed concentrations to emissions (e.g. Jiang *et al*. 2015; Yin *et al*. 2015 and refs therein).

Here we quantify CO emissions using version 8 multispectral total column CO observations from the NASA Terra MOPITT instrument (e.g. , Deeter *et al*. 2019) and a 4D variational adjoint approach based on the GEOS-Chem global chemical transport model (Henze *et al*. 2007, Appendices 1 and 2). The approach we use is similar to and builds from previous work described in Jiang *et al*. (2017) and Worden *et al*. (2017) which also quantified CO emissions and used them for evaluating decadal changes in fire emissions of CH_4 and CO. Yearly, *a priori* for the fire emissions are from the GFED4s (van der Werf et al., 2017) data base and span the time series shown in the figure. All other combustion emissions for the *a priori* are fixed as they are from a combination of sources that do not span the time period shown (Table A2).

The upper right panel of Figure 1 shows the change in CO emissions for the time period corresponding to the observed changes in AOD in the bottom left panel. These results are consistent with previous studies using the MOPITT CO record (Jiang *et al*. 2015; Yin *et al*. 2015). As seen by visually comparing the top right and bottom left panel of Figure 1, many of the changes in CO emissions are found to be of the same sign and in the same regions as changes in MISR small-mode AOD.

In order to determine to what extent changes in small-mode AOD are related to changes in CO emissions we first update the primary aerosol emission precursors (Tables A2 and A3) by multiplying their emissions at each grid box by the ratio of the posterior to prior CO emissions. Aerosols (and AOD) are then computed either directly from the emissions or through secondary aerosol formation within the GEOS-Chem model. While we can attribute CO emissions to fires with this approach because most biomass burning has distinct seasonality and is straightforward to identify using other metrics such as burned area, we cannot unequivocally partition CO emissions into other combustion sources such as the energy and transport sector or to biogenic sources using this approach. However, previous studies indicate that the CO emissions in most industrialized countries are related to burning of fossil fuels and that biogenic emissions and oxidation of atmospheric hydrocarbons do not vary as much as the other sources (e.g. Jiang *et al*. 2015; H. Worden *et al*. 2019). This approach assumes that aerosols are tied either directly to combustion emissions such as through a change to cleaner burning, more efficient fuels, or that their changes are indirectly related by, for example, co-temporaneous policy directives that reduces aerosols while increasing combustion efficiency, or alternatively through changes in activity. The model AOD accounts for the column-wise integration of the MISR instrument and the sample time of the sun-synchronous orbit (Appendix-3). The modeled change in small-mode AOD is shown in the bottom right panel of Figure 1. Visual inspection confirms similar changes in both observed and modeled small-mode AOD in many of the high-emitting areas (labeled in bottom right panel).

We next compare in more detail the mean estimates of small-mode AOD and corresponding observations in Figures 2 and 3 for the regions labeled in Figure 1 (bottom right panel). Figure 2 shows a comparison for the industrial regions of the USA, Europe, India, and China between the modeled and observed small-mode AOD changes depicted in Figure 1. These comparisons show that observed and modeled trends are consistent within the uncertainties for the USA, Europe, and China and that the direct emission of small-mode aerosols from combustion explains the interannual to decadal changes in these aerosols. However, CO emissions and corresponding small-mode AOD over India do not show much of a trend, likely because of challenges in quantifying emissions in this region due to complexities in

atmospheric transport (e.g., Worden *et al*. 2010; Liu *et al*. 2010; Jiang *et al*. 2013; Jiang *et al*. 2015). In addition, the posterior emissions better capture the decadal variability relative to the prior as shown in Table 1. For example, the MISR observed small-mode AOD difference between the two decades for E. China is -0.031 ± 0.022, in agreement with the updated modeled emissions difference of -0.038 ± 0.0018.

Figure 3 shows a comparison of modeled small-mode AOD from fires against MISR observed small-mode AOD in regions that have high biomass burning as indicated by burned area. These comparisons are again consistent between the model and observation within the uncertainty levels. We find that small-mode AOD based on CO emissions shows substantial improvement in the inter-annual variability (IAV) as demonstrated by the improved correlations. Notably, the decadal changes in small-mode AOD are consistent with previous observations of a decline in fires in S. America and Indonesia (e.g., Andela *et al*. 2017, Worden *et al*. 2017). Table 1 also shows the decadal differences for the regions dominated by fire emissions. In contrast to the improved agreement in IAV found for the anthropogenic regions where the prior emission is fixed, there is not much improvement in these comparisons where the prior emission is annually set, likely because the trends in burned area are similar to prior CO emissions in these regions (Worden *et al*. 2017).

We next test if changes in meteorology can also explain the small-mode AOD variability by performing a model run with fixed emissions (Appendix 4) and find that changes in dynamics cannot explain the observed variability in small-mode AOD. Variations in biogenic emissions may play a role in tropical regions, however these variations are small relative to variations in biomass burning in these same regions (Jiang *et al*. 2015; H. Worden *et al*. 2019). Other confounding factors are the large uncertainties in aerosol formation, the partitioning of these sources and how both combustion and non-combustion sources affect AOD. Uncertainties from these other factors cannot be easily calculated due to computational challenges and poor knowledge about their uncertainty characteristics. Hence our result that for the non-fire sector that small-mode AOD is correlated with CO emissions should be taken as purely empirical with additional analysis needed to relate observed variability to specific emissions.

3. Discussion and Implications

Decreasing both aerosol and CO emissions can be accomplished in multiple ways, both directly and indirectly, and need not be causally related. We expect a concurrent change in CO emissions and small-mode AOD for fire emissions as both are released during combustion (e.g., van der Werf 2010, 2017;

Worden *et al*. 2017; Andela *et al*. 2017). A switch from coal to natural gas also results in both reduced aerosols and improved combustion efficiency resulting in lower CO emissions (e.g., Burney 2020, Buchholz et al., 2021); however, we do not attempt to estimate how much of the observed change in small-mode AOD across the globe is due to this coal-to-gas fuel transition and leave this to a subsequent study. On the other hand, policies implemented contemporaneously that result in improved filtering of aerosols and increased combustion efficiency such as for from coal-powered plants (Karplus *et al*. 2017; Lu *et al*. 2020) and other combustion sources such as from traffic can result in the same outcome of reduced AOD and CO emissions. Changes in agricultural CO and aerosol emissions may also be correlated entirely through activity (Warner *et al*. 2017) as aerosol pre-cursors from fertilizer use, as well as the corresponding dust and combustion associated with farming can occur in tandem. Nonetheless, the empirical observation shown here that changes in small-mode AOD are well correlated with changes in CO emissions in N. America, Europe, and Asia suggest a link between the two that should be tested in subsequent studies; this would require more in-depth analysis between the different emission sectors and aerosol emissions. We note that these changes in emission do not necessarily reflect a decrease or increase in carbon dioxide except in fire-prone regions but instead reflects a change in combustion efficiency as overall CO_2 levels continue to increase during this time period (Friedlingstein *et al*. 2019).

The decline in observed small-mode AOD in N. America, Europe, China, and S. America has implications for air quality in these regions as they are correlated with near-surface aerosols and subsequently with PM 2.5 concentrations (e.g., Donkelaar *et al*. 2015). To quantify these effects, we show (Figure 4) the modeled surface PM2.5 concentrations and its changes that correspond to aerosl and CO emission changes shown in Figures 1 through 3. The top left panel of Figure 4 shows the mean PM2.5 concentration from all sources based on the GEOS-Chem model. Largest values of PM2.5 concentrations from are in desert regions and are due to fine-mode mineral dust (e.g., Bauer *et al*. 2019). The top right panel shows the net change in PM2.5 globally whereas the bottom panels show the changes for the industrial (bottom left) and fire prone (bottom right) regions. The sign of these changes is consistent with a number of local and regional studies using ground-based data. The biggest improvement in the magnitude of PM2.5 is in China, consistent with Lu *et al*. (2020 and refs therein) with smaller changes in the magnitude of PM2.5 in N. America (e.g. Bennett *et al*. 2019). The decline of PM2.5 in Europe and slight increase in E. Australia are consistent with observed changes in PM2.5 in corresponding urban locations (e.g. de Jesus *et al*. 2020). The increase in Indonesia is driven almost entirely by the 2015 ENSO related fires but if these are removed there is a small decrease. Exact comparisons between these model based (but data constrained) estimates of

surface PM2.5 decadal changes and local surface measurements are challenging because of the difference in scales between the measurements. Nonetheless, these results indicate that a reduction in combustion related air-quality emissions in these areas have improved the air quality. However, the climate impacts of these changes are uncertain as this study is not able to determine if there has been a shift from sulfate aerosols, which mainly scatter radiation, to black carbon aerosols, which also absorbs radiation. A shift to black carbon, even as aerosols are reduced, could have negative climate impact due to the increased atmospheric heating even if there is a reduced radiation transferred to the surface (e.g. Haywood and Ramaswamy 1998; Ramanathan et al. 2001, 2005, Streets *et al*. 2006 and refs therein).

Acknowledgements

This research was carried out at the Jet Propulsion Laboratory, California Institute of Technology under a contract with National Aeronautics and Space Administration (80NM0018D0004). We acknowledge the funding support by the JPL Strategic Advances in Air Quality Research and Technology Development. We also thank the support from NASA ROSES ACMAP and TASNPP programs.

Data Statement

The satellite data used in this study are publicly available for download at NASA website https://earthdata.nasa.gov/about/daacs. In addition, websites available for data download include: MOPITT level 2 data products: ftp://15ftl01.larc.nasa.gov/MOPITT/MOP02J.008; MISR level 2 data products: ftp://l5ft101.larc.nasa.gov/MISR. All data underlying this article are available in the article. For additional questions regarding the data sharing and data assimilation system, please contact the corresponding author at John.R.Worden@jpl.nasa.gov.

Author contributions

J.W., M.L., and J.J. designed the research; M. L performed the CO flux inversion, AOD model simulation, and comparison of the modeled AOD with the MISR-AOD. J.W and M.L wrote the manuscript and the co-authors assisted in manuscript preparation. Several co-authors are also involved in evaluating the results and preparing the data needed for this research. These include B.B. for ATom CO comparison, M. W. for MISR AOD mode properties, and K. M. for OH, SO_2, and NOx data products.

244

245 **Appendix**

246

247 ***A.1 GEOS-Chem emission inventories.***

248 We organize emission inventories for CO and aerosols integrating anthropogenic, biofuel,
249 biogenic, and fire emission sources. For the non-fire emission sources, a combination of global
250 and regional emission inventories are used in this study (Table A2). The global models include
251 EDGAR (Olivier and Berdowski, 2001), Global Emission InitAtive (GEIA) (A.F. Bouwman,
252 1997), and Bond (T.C. Bond et al 2007). The regional models include the US Environmental
253 Protection Agency (EPA) National Emission Inventory (NEI) for 2008 in North America, the
254 Criteria Air Contaminants (CAC) inventory for Canada, the Big Bend Regional Aerosol and
255 Visibility Observational (BRAVO) Study Emissions Inventory for Mexico (Kuhns et al.,2003),
256 the Cooperative Program for Monitoring and Evaluation of the Long-range Transmission of Air
257 Pollutants in Europe (EMEP) inventory for Europe in 2000 (Vestreng and Klein, 2002) and the
258 Streets Asia emissions inventory for 2000. For the biogenic emission type, we employ the Model
259 of Emissions of Gases and Aerosols from Nature, version2.1 (MEGAN; Guenther et al., 2012)
260 and MERRA 2 meteorology to derive CO and OC emissions and integrate the off-line emission
261 inventory from GEIA for NH3. For fire emission, we derive emissions for the above five
262 constituents based on the dry mass GFED4s (van der Werf et al., 2017).
263 We prepare the non-fire emission inventories only for a single year due to limited temporal
264 coverage of the emission datasets described above. For the fire emission, we prepare a single
265 year inventory for the first decade (2002-2009) but annual inventories for the second decade. All
266 emission datasets are at 2°x2.5° spatial resolution with 3 hourly temporal resolution. The total
267 emission budget integrating the non-fire and the fire emissions are shown for different regions in
268 Table A2.

269

270 ***A.2 Adjoint model based 4DVAR Assimilation Process***.

271 We use the Greenhouse Gas Framework – Flux (GHGF-Flux) 4D-Var assimilation system
272 for CO flux inversions. This system has been developed under the NASA Carbon Monitoring
273 System (CMS) project and inherits the chemistry transport model and adjoint model from the

GEOS-Chem adjoint (Liu et al., 2020; Byrne et al., 2020). We drive the chemical transport by the Modern-Era Retrospective Analysis for Research and Applications, Version 2 (MERRA-2) meteorology products. For OH field, we combine the tropospheric-OH data products obtained from the TCR-2 framework (Miyazaki et al., 2020) and the stratospheric OH data products from the Global Modeling Initiative (GMI, https://gmi.gsfx.nasa.gov) of the NASA Modeling Analysis and Prediction Program.

The 4D-Var data assimilation system minimizes a cost function which is defined as

$$J(x) = \sum_{i=1,N} (F_i(x) - y_i)^T R^{-1} (F_i(x) - y_i)) + (x - x_a)^T B^{-1} (x - x_a)$$

where x is the state vector of CO emission, N is the number of observations within the assimilation period, y is the observed state, F(x) is the forward model, and R and B are variance of the observed state and the prior CO emission. We optimize a scaling factor array applied to the prior CO emission with the assimilation window of one month. We sequentially perform the monthly assimilation process generating the initial condition of the succeeding month based on the optimized CO emission. For the assimilation process, we organize prior CO emissions integrating emissions from anthropogenic, biogenic, and fire emission sources.

To evaluate the fidelity of the CO emission estimates, we compare the prior and the posterior CO concentrations against in-situ CO measurements. Figure 5 and 6 show the comparison against the surface flask measurements and the NASA's Atmospheric Tomography Mission (ATOM). The surface flask measurements are typically over continental regions whereas the ATOM data are typically over the ocean. Both sets of comparisons show improvement between prior and posterior as compared to these data sets.

A.3 Aerosol Emission Inventories and AOD Change Estimation.

The AOD is a function of the aerosol concentration and the particle properties of the aerosol type. We simulate AOD and the surface PM2.5 from sulfate aerosols and carbonaceous aerosols to compare with the small mode MISR-AOD. In GEOS-Chem, the sulfate aerosol tracers include SO_4, ammonia (NH_4), and Nitrate (NIT) and the carbonaceous aerosol tracers include hydrophilic black carbon (BCPI), hydrophobic black carbon (BCPO), hydrophilic organic carbon (OCPI), and hydrophobic organic carbon (OCPO). The SO_4 emission is derived as a fraction of the SO2

emission, 3% globally, 5% over USA, and 1.3 % over Europe and the BC and OC emissions are shared between the hydrophobic and hydrophilic carbonaceous aerosols, 20 % and 80%, respectively. The gas-to-particle reactions of the sulfate aerosols (Metzger et al, 2002) involve SO_4, NH_3, and HNO_3. We integrate the tropospheric-NOx emissions from the TCR-2 framework for HNO_3 concentration simulation.

To estimate the AOD changes due to the combustion emissions, we update the prior aerosol emissions of BC, OC, and SO_2 (Appendix 1) with the optimal emission scale factors obtained from the MOPITT-CO assimilation (Appendix 2). The posterior aerosol emissions (i.e., updated prior aerosol emissions) provide a full coverage between 2002 and 2019 for the anthropogenic, biofuel, and biogenic emission types following the posterior CO emission trend. The fire emissions for BC, OC, SO_2, and NH_3 are computed based on the updated dry mass and the corresponding emission factors. Note that the posterior NH_3 emission is updated only for the fire emission type, consequently changes in agriculture and livestock which also affect NH_3 emissions (Warner *et al*. 2017; van Damme *et al*. 2018) are not included in the estimated AOD changes shown in Figure 1. Table A4 lists the decadal mean (average of the annual mean over a decade) of the posterior emission inventories of CO, BC, OC, SO_2, and NH_3.

A.4 AOD variations for constant emission scenario

Variations in wind fields, humidity, and temperature all affect aerosol emission and subsequent AOD; in this study we test if changes in these environmental parameters can also explain changes to the observed AOD. The atmospheric dynamics model simulation requires the surface pressure, temperature, winds, planetary boundary layer height, cloud mass flux, and detrainment. The wet scavenging model simulation requires the relative humidity, precipitation, and rain water source. The dry deposition model simulation requires the surface temperature, the surface roughness, and the albedo. To test whether decadal variations in meteorology can explain observed small-mode AOD trends we run the AOD model simulation for the entire study time period keeping the emissions constant and changing only the meteorology fields. Figure 7 shows the results of this study and demonstrates the changes in environmental factors cannot explain observed decadal changes in AOD as AOD remains approximately constant for all regions for this scenario.

Table 1 Decadal trend of the MISR AOD, Prior AOD, and Posterior AOD

Region	AOD	Decade 1 (2002-2010)	Decade 2 (2011-2019)	Change (Decade2 – Decade1)
E China	MISR	0.19656 ± 0.00892	0.16575 ± 0.02093	-0.03081 ± 0.02275
	Prior	0.17979 ± 0.00429	0.17884 ± 0.00461	-0.00094 ± 0.00630
	Posterior	0.19315 ± 0.00935	0.15547 ± 0.01541	-0.03768 ± 0.01802
Europe	MISR	0.06031 ± 0.00506	0.05002 ± 0.00454	-0.01029 ± 0.00680
	Prior	0.05535 ± 0.00158	0.05530 ± 0.00173	-0.00006 ± 0.00234
	Posterior	0.05939 ± 0.00640	0.05239 ± 0.00285	-0.00700 ± 0.00700
India	MISR	0.13437 ± 0.00684	0.15358 ± 0.00648	0.01922 ± 0.00943
	Prior	0.09298 ± 0.00279	0.09168 ± 0.00183	-0.00130 ± 0.00333
	Posterior	0.08698 ± 0.00886	0.09201 ± 0.00357	0.00503 ± 0.00955
USA-East	MISR	0.08291 ± 0.00759	0.06393 ± 0.00882	-0.01898 ± 0.01164
	Prior	0.07511 ± 0.00182	0.07669 ± 0.00202	0.00158 ± 0.00272
	Posterior	0.07523 ± 0.00585	0.07061 ± 0.00653	-0.00462 ± 0.00877
Africa	MISR	0.14092 ± 0.00615	0.14544 ± 0.00502	0.00452 ± 0.00794
	Prior	0.11285 ± 0.00435	0.11669 ± 0.00355	0.00384 ± 0.00561
	Posterior	0.12460 ± 0.00687	0.12664 ± 0.00606	0.00204 ± 0.00916
Australia	MISR	0.04148 ± 0.00358	0.04336 ± 0.00355	0.00188 ± 0.00504
	Prior	0.02831 ± 0.00230	0.02807 ± 0.00339	-0.00024 ± 0.00410
	Posterior	0.04472 ± 0.00433	0.04241 ± 0.00592	-0.00231 ± 0.00733
Indonesia	MISR	0.06775 ± 0.01481	0.06894 ± 0.01853	0.00119 ± 0.02372
	Prior	0.04470 ± 0.00400	0.05689 ± 0.01662	0.01219 ± 0.01710
	Posterior	0.05695 ± 0.01427	0.06101 ± 0.02926	0.00406 ± 0.03256
S. America	MISR	0.07900 ± 0.01169	0.06838 ± 0.00894	-0.01062 ± 0.01472
	Prior	0.06406 ± 0.00859	0.05719 ± 0.00567	-0.00686 ± 0.01029
	Posterior	0.07288 ± 0.01077	0.05460 ± 0.00764	-0.01828 ± 0.01321

Table 1 lists the mean and variance of small mode MISR AOD, the model AOD computed with the prior aerosol emissions (prior), and the model AOD computed with the updated aerosol emissions by the ratio of the CO posterior to prior emission (posterior) for two decades. The change column shows the mean value change between the two decades with the uncertainty computed as the root mean square of the respective variances.

Table A*2* Prior Emission Inventory Organization

Emission type	Emission model	CO Tg CO /year	BC Tg C /year	OC Tg C /year	SO_2 Tg SO_2 /year	NH_3 Tg NH_3 /year
Anthropogenic	EDGAR + regional	470 (0.37)			29.69 (0.95)	32.51 (0.64)
	Bond		2.98 (0.49)	3.05 (0.10)		
Biofuel	GEIA	232 (0.18)			0.27 (0.01)	1.61 (0.03)
	Bond		1.55 (0.26)	6.28 (0.20)		
Biogenic	MEGAN	235 (0.18)	0.0	8.97 (0.29)	0.0	
	GEIA					14.26 (0.28)
Fire (mean)	GFED4	333 (0.26)	1.53 (0.25)	12.86 (0.41)	0.96 (0.03)	2.67 (0.05)
Total		1270 (1.00)	6.05 (1.00)	31.17 (1.00)	30.92 (1.00)	51.05 (1.00)

Table A2 lists the emissions from the prior emission inventories for CO, BC, OC, SO_2, and NH_3 with respect to four emission types (anthropogenic, biofuel, biogenic, and fire) and the contribution (fraction) of each emission type to the total emission budget in parentheses. The emission models within each emission type represent the provenance of the emission data products or derivation processes (e.g., MEGAN and GFED4).

Table A3 Global and Regional Anual Budget of Prior Emissions

	CO (TgCO /year)	**BC** (Tg C/year)	**OC** (Tg C/year)	**SO_2** (Tg SO_2 /year)	**NH_3** (Tg NH_3/year)
Global	1270	6.05	31.17	30.92	51.05
Anthropogenic regions					
USA-east	35.51	0.17	0.49	2.95	1.15
Europe	27.90	0.32	0.50	1.45	2.92
India	115.53	0.49	1.57	1.57	6.29
China	152.53	0.98	2.00	6.20	4.74
Fire regions					
Africa	164.86	0.80	6.02	0.84	2.68
Indonesia	78.23	0.23	1.77	1.65	1.35
S. America	140.63	0.33	3.85	2.21	2.89
Australia	32.78	0.11	0.99	1.30	0.99

Table A3 lists the global emission budget (Total emission in Table A2) and regional distribution in the four anthropogenic regions and the four fire regions shown in Figure 1.d.

381

382

383 **Table A4 Decadal Comparison of Posterior Emissions**

	CO (Tg CO/year)		**BC** (Tg C/year)		**OC** (Tg C/year)		**SO_2** (Tg SO_2 /year)		**NH_3** (Tg NH_3 /year)	
Decade	1	2	1	2	1	2	1	2	1	2
globe	1592	1465	8.02	7.30	37.61	36.30	42.88	36.41	51.05	50.72
Anthropogenic regions										
USA-east	56	47	0.33	0.27	0.91	0.78	5.9	4.50	1.15	1.15
Europe	52	45	0.61	0.52	0.95	0.84	2.44	2.16	2.92	2.92
India	92	93	0.42	0.42	1.33	1.32	1.45	1.47	5.46	5.46
China	149	113	1.11	0.84	2.23	1.68	6.86	5.18	4.86	4.86
Fire regions										
Africa	179	189	0.87	0.93	6.38	6.77	0.99	1.08	3.77	3.99
Indonesia	55	52	0.24	0.21	1.51	1.51	1.86	1.57	1.42	1.25
S. America	153	121	0.43	0.33	4.03	3.13	2.37	2.27	3.46	3.12
Australia	63	67	0.23	0.22	1.87	2.08	1.99	1.99	1.54	1.56

384

385 Table A4 compares the average annual budget of the posterior emissions of CO, BC, OC, SO_2,
386 and NH_3 between the first decade (2002-2009) and the second decade (2010-2019), globally and
387 regionally. Note that the NH_3 posterior emission is updated only for the fire emission type.

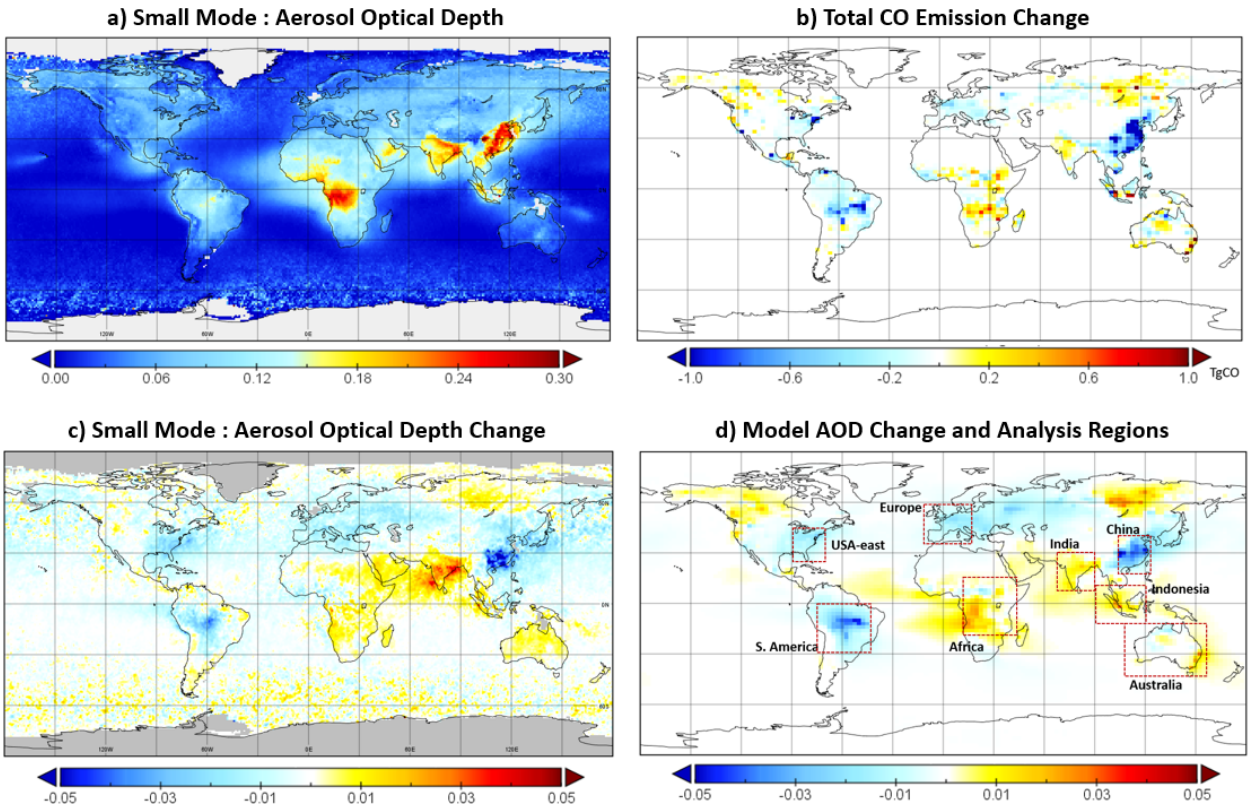

Figure 1. Relationships between combustion emissions and AOD of the small size aerosols (< 0.7 um in diameter) during the two decades (2002-2019): (a) average of the annual mean AOD over two decades of the small-mode MISR-AOD, (b) decadal change of the total CO emission annual budget, (c) decadal change of the small-mode MISR-AOD, and (d) decadal change of the model-AOD with an overlay of the eight study regions, where the decadal change refers to the average of the annual mean over the second decade minus the average of the annual mean over the first decade. Figure 1.d overlays the eight study regions selected for the annual trend investigation, four regions with a high level of anthropogenic pollution (China, India, Europe, and eastern USA) and four regions with a high level of wild-fire events (South America, Africa, Indonesia, and Australia).

Figure 2. Comparison of small-mode MISR AOD, model AOD computed with the prior aerosol emission (prior), and model AOD computed with the posterior aerosol emission (posterior) in four anthropogenic regions (Figure 1.d). The R value represent the correlation between the model AOD and the small-mode MISR-AOD and the E value are the root mean square difference between the model AOD and the small-mode MISR-AOD.

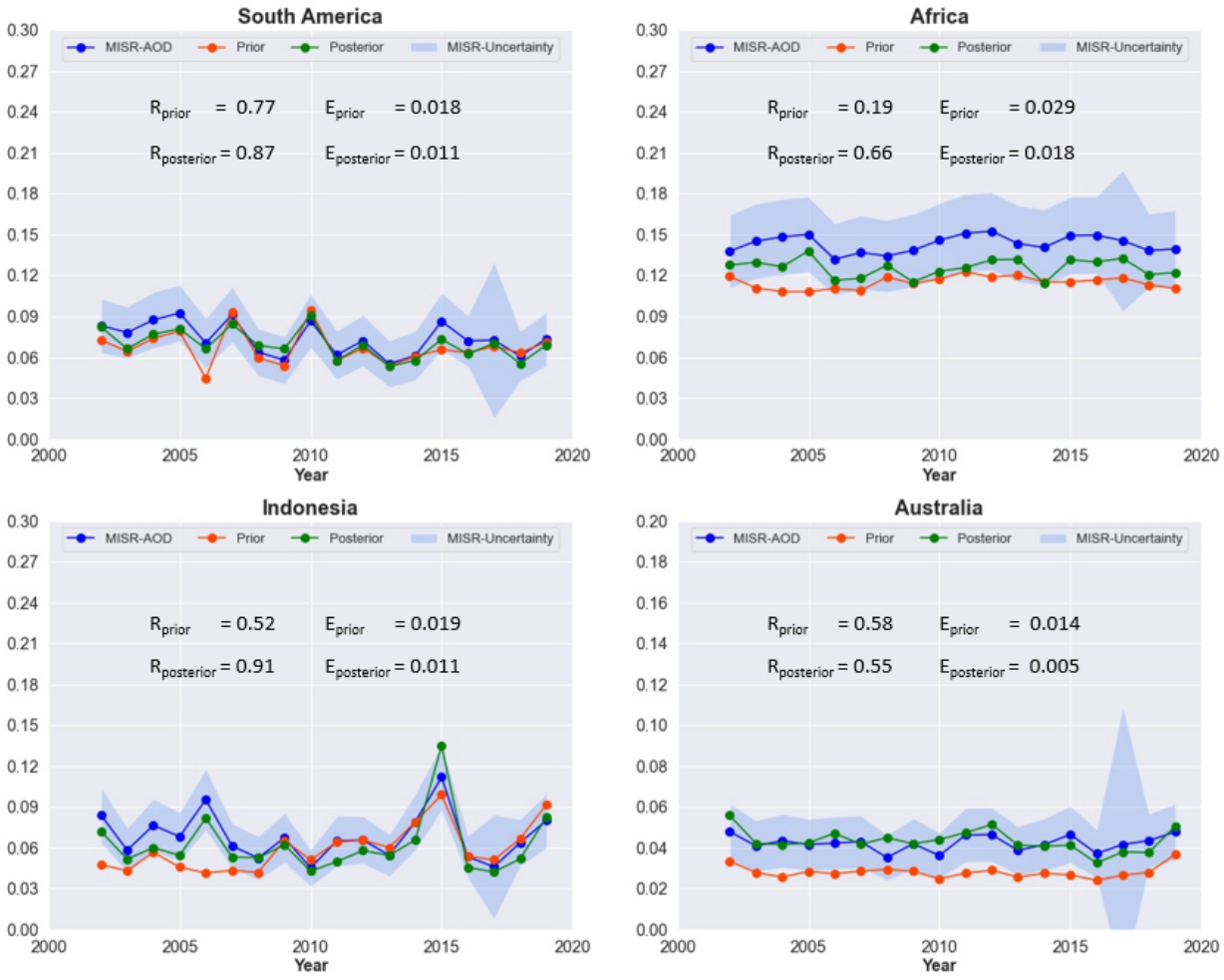

Figure 3. Comparison of small-mode MISR AOD, model AOD computed with the prior aerosol emission (prior), and model AOD computed with the posterior aerosol emission (posterior) in four wildfire dominant regions (Figure 1.d). The R value represent the correlation between the model AOD and the small-mode MISR-AOD and the E value are the root mean square difference between the model AOD and the small-mode MISR-AOD.

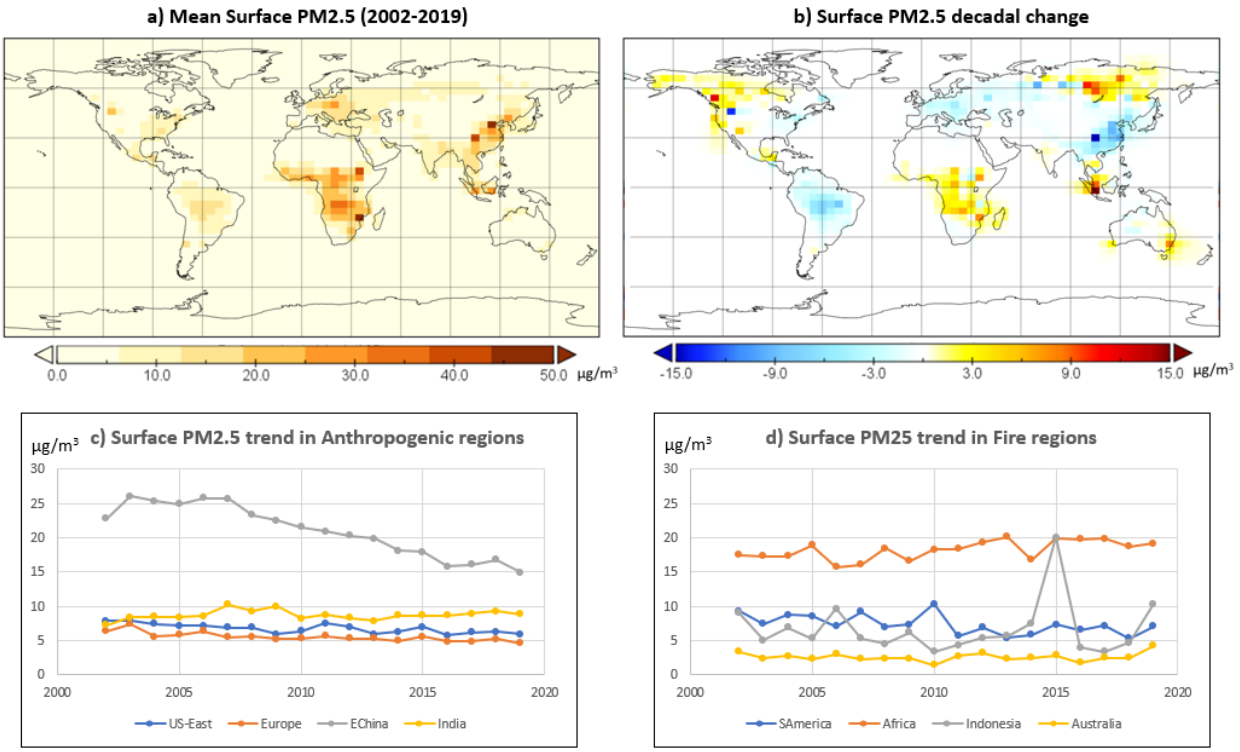

Figure 4. Model surface-PM2.5 a) annual mean averaged over two-decades (2002-2019), b) change (second decade – first decade) between the first decade (2002-2009) and the second decade (2010-2019), (c) comparison of the annual trend in four anthropogenic regions (Figure 1.d) , (d) comparison of the annual trend in four wild fire dominated regions (Figure 1.d).

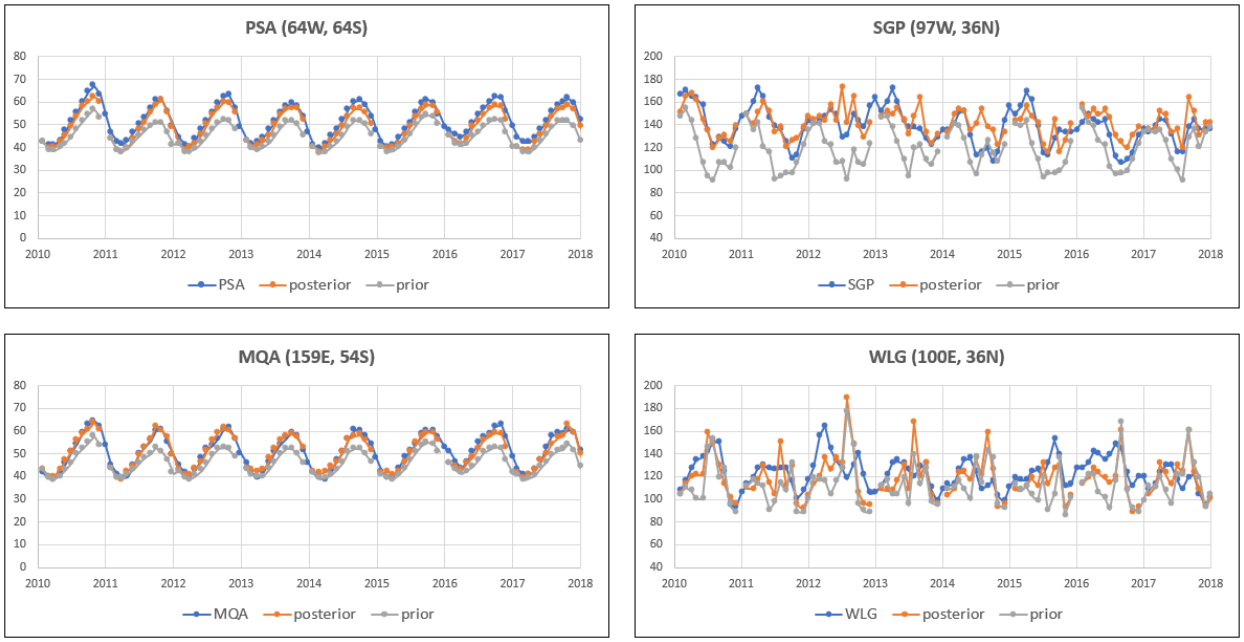

Figure 5. Comparison of the monthly surface CO concentration between surface flask measurements, model surface concentration simulated with the prior CO emission (prior), and model surface concentration simulated with MOPITT-CO constrained CO emission (posterior). These four regions were chosen as they were the only sites that provide a complete record over the study period.

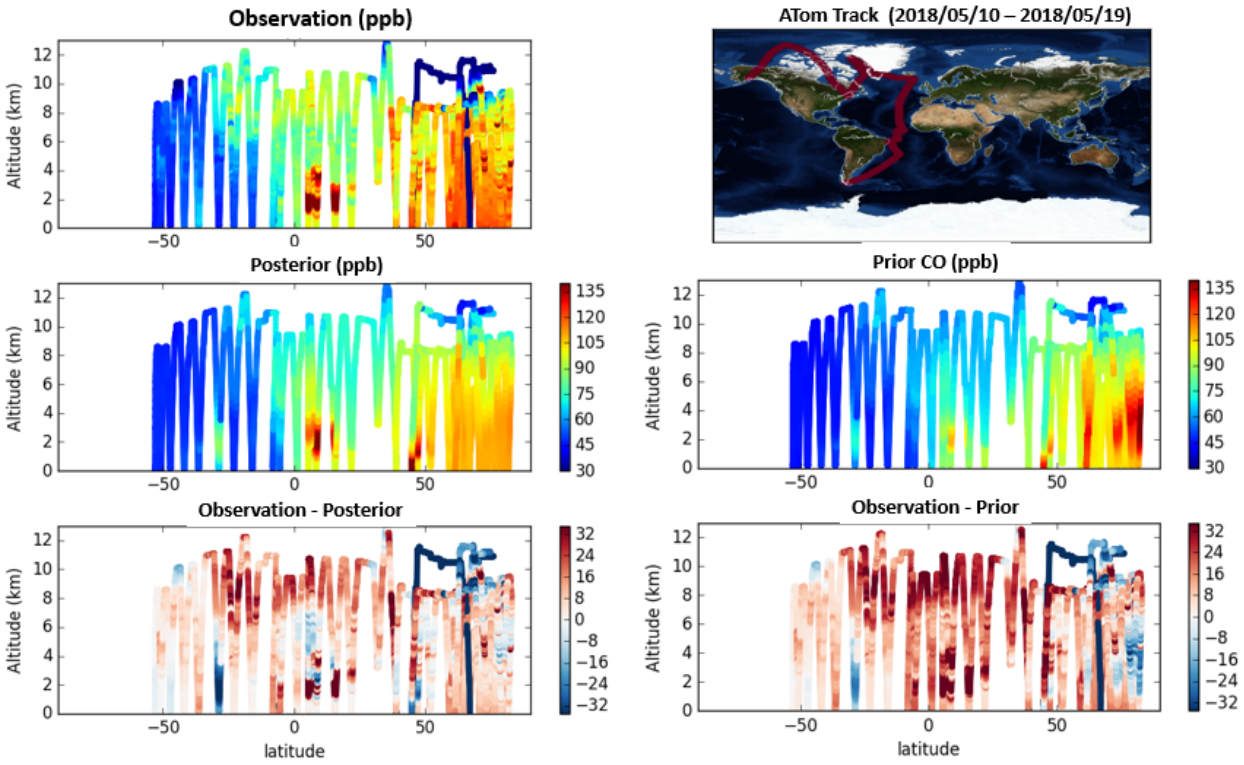

Figure 6. Comparison of the profile CO concentration between the aircraft measurements from NASA's Atmospheric Tomography Mission (ATom), model concentration profile simulated with the prior CO emission (prior) and model concentration profile computed with the MOPITT-CO constrained CO emission (posterior).

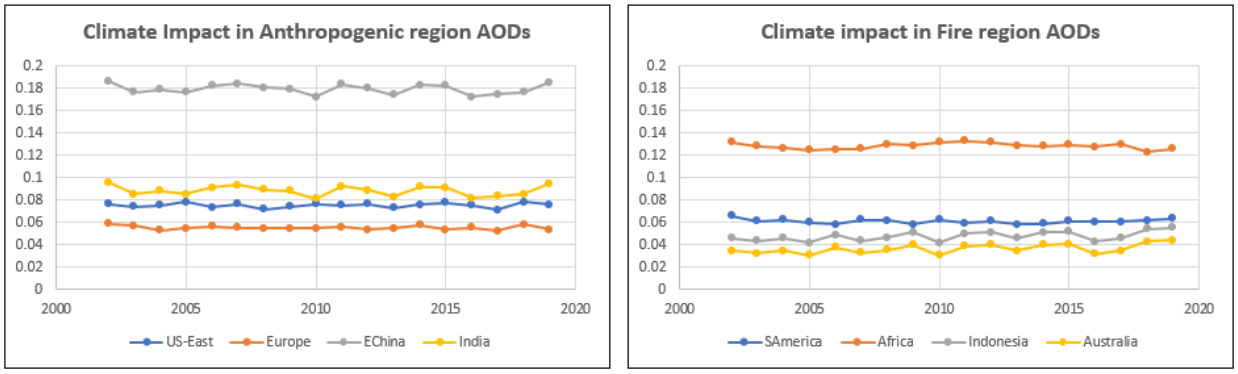

Figure 7. Modeled AOD trends in four anthropogenic and four wildfire dominated regions for a constant emission scenario.

References

Andela, N. et al. (2017), A human-driven decline in global burned area, *Science*, *356*, 1356–1362, doi:10.1126/science.aal4108.

Andreae, M. O., D. Rosenfeld, P. Artaxo, A. A. Costa, G. P. Frank, K. M. Longo, and M. Silva-Dias (2004), Smoking rain clouds over the Amazon, *Science*, *303*(5662), 1337–1342.

Bauer, S. E., U. Im, K. Mezuman, and C. Y. Gao (2019), Desert Dust, Industrialization, and Agricultural Fires: Health Impacts of Outdoor Air Pollution in Africa, *Journal of Geophysical Research-Atmospheres*, *124*(7), 4104–4120, doi:10.1029/2018JD029336.

Bennett, J. E., H. Tamura-Wicks, R. M. Parks, R. T. Burnett, C. A. Pope III, M. J. Bechle, J. D. Marshall, G. Danaei, and M. Ezzati (2019), Particulate matter air pollution and national and county life expectancy loss in the USA: A spatiotemporal analysis, *PLOS Medicine*, *16*(7), e1002856, doi:10.1371/journal.pmed.1002856.

Bouwman, A.F., D. S. Lee, W. A. H. Asman, et al, A global high-resolution emission inventory for ammonia, Global Biogeochemical Cycles, Vol. 11, No. 4, 561-587, 1997

Buchholz, R. R., Worden, H. M., Park, M., et al., Air pollution trends measured from Terra: CO and AOD over industrial, fire-prone, and background regions, Remote Sensing of Environment, Accepted December 2020.

Burney, J. A. (2020), The downstream air pollution impacts of the transition from coal to natural gas in the United States, *Nature Sustainability*, 1–19, doi:10.1038/s41893-019-0453-5.

Byrne, B., Liu, J., Lee, M., Baker, I., Bowman, K. W., Deutscher, N. M., et al. (2020). Improved constraints on northern extratropical CO2 fluxes obtained by combining surface-based and space-based atmospheric CO2 measurements. Journal of Geophysical Research: Atmospheres, 125, e2019JD032029. https://doi.org/10.1029/2019JD032029

Dedoussi, I. C., S. D. Eastham, E. Monier, and S. R. H. Barrett (2020), Premature mortality related to United States cross-state air pollution, *Nature*, 1–19, doi:10.1038/s41586-020-1983-8.

Deeter, M. N., D. P. Edwards, G. L. Francis, J. C. Gille, D. Mao, S. Martinez-Alonso, H. M. Worden, D. Ziskin, and M. O. Andreae (2019), Radiance-based retrieval bias mitigation for the MOPITT instrument: the version 8 product, *Atmos. Meas. Tech.*, *12*(8), 4561–4580, doi:10.5194/amt-12-4561-2019.

Dey, S., and L. Di Girolamo (2011), A decade of change in aerosol properties over the Indian subcontinent, *Geophys. Res. Lett*, *38*(14), n/a–n/a, doi:10.1029/2011GL048153.

DSc, D. A. J. C. et al. (2017), Estimates and 25-year trends of the global burden of disease attributable to ambient air pollution: an analysis of data from the Global Burden of Diseases Study 2015, *The Lancet*, *389*(10082), 1907–1918, doi:10.1016/S0140-6736(17)30505-6.

Friedlingstein, P. et al. (2019), Global Carbon Budget 2019, *Earth Syst. Sci. Data*, *11*(4), 1783–1838, doi:10.5194/essd-11-1783-2019.

Haywood, J. M., and V. Ramaswamy (1998), Global sensitivity studies of the direct radiative forcing due to anthropogenic sulfate and black carbon aerosols, *Journal of Geophysical Research: Atmospheres*, *103*(D6), 6043–6058, doi:10.1029/97JD03426.

Henze, D. K., A. Hakami, and J. H. Seinfeld (2007), Development of the adjoint of GEOS-Chem, *Atmospheric Chemistry and Physics*, *7*(9), 2413–2433.

Hilboll, A., A. Richter, and J. P. Burrows (2013), Long-term changes of tropospheric NO₂ over megacities derived from multiple satellite instruments, *Atmospheric Chemistry and Physics*, *13*(8), 4145–4169, doi:10.5194/acp-13-4145-2013.

Huang, R.-J. et al. (2014), High secondary aerosol contribution to particulate pollution during haze events in China, *Nature*, 1–5, doi:10.1038/nature13774.

491 Jaeglé, L., P. K. Quinn, T. S. Bates, B. Alexander, and J. T. Lin (2011), Global distribution of
492 sea salt aerosols: new constraints from in situ and remote sensing observations, *Atmospheric*
493 *Chemistry and Physics*, *11*(7), 3137–3157, doi:10.5194/acp-11-3137-2011.

494 Jiang, J. H., H. Su, L. Huang, Y. Wang, S. Massie, Bin Zhao, A. Omar, and Z. Wang (2018),
495 Contrasting effects on deep convective clouds by different types of aerosols, *Nat Commun*,
496 1–7, doi:10.1038/s41467-018-06280-4.

497 Jiang, Z., D. B. A. Jones, H. M. Worden, M. N. Deeter, D. K. Henze, J. Worden, K. W.
498 Bowman, C. A. M. Brenninkmeijer, and T. J. Schuck (2013), Impact of model errors in
499 convective transport on CO source estimates inferred from MOPITT CO retrievals, *Journal*
500 *of Geophysical Research-Atmospheres*, *118*(4), 2073–2083, doi:10.1002/jgrd.50216.

501 Jiang, Z., J. R. Worden, H. Worden, M. Deeter, D. B. A. Jones, A. F. Arellano, and D. K. Henze
502 (2017), A 15-year record of CO emissions constrained by MOPITT CO observations,
503 *Atmospheric Chemistry and Physics*, *17*(7), 4565–4583, doi:10.5194/acp-17-4565-2017-
504 supplement.

505 Jimenez, J. L., M. R. Canagaratna, and N. M. Donahue (2009), Evolution of organic aerosols in
506 the atmosphere, *science.sciencemag.org*, *326*, doi:10.1126/science.1179518.

507 Kahn, R. A., B. J. Gaitley, M. J. Garay, D. J. Diner, T. F. Eck, A. Smirnov, and B. N. Holben
508 (2010), Multiangle Imaging SpectroRadiometer global aerosol product assessment by
509 comparison with the Aerosol Robotic Network, *J. Geophys. Res*, *115*(D23), D23209,
510 doi:10.1029/2010JD014601.

511 Karplus, V. J., S. Zhang, and D. Almond (2018), Quantifying coal power plant responses to
512 tighter SO2 emissions standards in China, *Proceedings of the National Academy of Sciences*
513 *of the United States of America*, *115*(27), 7004–7009, doi:10.1073/pnas.1800605115.

514 Kaufman, Y. J., I. Koren, L. A. Remer, D. Rosenfeld, and Y. Rudich (2005), The effect of
515 smoke, dust, and pollution aerosol on shallow cloud development over the Atlantic Ocean,
516 *Proceedings of the National Academy of Sciences of the United States of America*, *102*(32),
517 11207–11212, doi:10.1073/pnas.0505191102.

518 Koren, I., O. Altaratz, L. A. Remer, G. Feingold, J. V. Martins, and R. H. Heiblum (2012),
519 Aerosol-induced intensification of rain from the tropics to the mid-latitudes, *Nature*
520 *Geoscience*, *5*(2), 118–122, doi:10.1038/ngeo1364.

521 Krotkov, N. A. et al. (2016), Aura OMI observations of regional SO₂
522 and NO₂ pollution changes from 2005 to 2015, *Atmospheric*
523 *Chemistry and Physics*, *16*(7), 4605–4629, doi:10.5194/acp-16-4605-2016.

524 Kuhns, H., Green, M., and Etyemezian, V.: Big Bend Regional Aerosol and Visibility
525 Observational (BRAVO) Study Emissions Inventory, Report prepared for BRAVO Steering
526 Committee, Desert Research Institute, Las Vegas, Nevada, 2003.

527 Liao, H., D. K. Henze, J. H. Seinfeld, S. Wu, and L. J. Mickley (2007), Biogenic secondary
528 organic aerosol over the United States: Comparison of climatological simulations with
529 observations, *J. Geophys. Res*, *112*(D6), 13791–1, doi:10.1029/2006JD007813.

530 Liu, J. J., D. B. A. Jones, J. R. Worden, D. Noone, M. Parrington, and J. Kar (2009), Analysis of
531 the summertime buildup of tropospheric ozone abundances over the Middle East and North
532 Africa as observed by the Tropospheric Emission Spectrometer instrument, *J. Geophys. Res*,
533 *114*(D5), D05304, doi:10.1029/2008JD010993.

534 Lu, X., S. Zhang, J. Xing, Y. Wang, W. Chen, D. Ding, Y. Wu, S. Wang, L. Duan, and J. Hao
535 (2020), Progress of Air Pollution Control in China and Its Challenges and Opportunities in
536 the Ecological Civilization Era, *Engineering*, 1–9, doi:10.1016/j.eng.2020.03.014.

537 de Jesus, A. L. et al. (2020), Long-term trends in PM2.5 mass and particle number
538 concentrations in urban air: The impacts of mitigation measures and extreme events due to
539 changing climates, *Environmental Pollution*, *263*(Part A), 114500,
540 doi:10.1016/j.envpol.2020.114500.

541 Mehta, M., R. Singh, A. Singh, N. Singh, Anshumali (2016), Recent global aerosol optical depth
542 variations and trends — A comparative study using MODIS and MISR level 3 datasets,
543 *Remote Sensing of Environment*, *181*(C), 137–150, doi:10.1016/j.rse.2016.04.004.

544 Metzger, S., Dentener, F., Pandis, S., and Lelieveld, J (2002), Gas/aerosol partitioning: 1. A
545 computationally efficient model, J. Geophys. Res.-Atmos., 107, 4312,
546 doi:10.1029/2001JD001102.

547 Miyazaki, K., Eskes, H., Sudo, K., Boersma, K. F., Bowman, K., and Kanaya, Y.: Decadal
548 changes in global surface NO_x emissions from multi-constituent satellite data assimilation,
549 Atmos. Chem. Phys., 17, 807–837, https://doi.org/10.5194/acp-17-807-2017, 2017.

550 Olivier, J. G. J. and Berdowski, J. J. M.: Global emissions sources and sinks, in: The Climate
551 System, edited by: Berdowski, J., Guicherit, R., and Heij, B. J., A. A. Balkema
552 Publishers/Swets & Zeitlinger Publishers, Lisse, the Netherlands, 33–78, 2001

553 Ramanathan, V. et al. (2001), Indian Ocean Experiment: An integrated analysis of the climate
554 forcing and effects of the great Indo-Asian haze, *Journal of Geophysical Research-*
555 *Atmospheres*, *106*(D22), 28371–28398, doi:10.1029/2001JD900133.

556 Ramanathan, V., C. Chung, D. Kim, T. Bettge, L. Buja, J. T. Kiehl, W. M. Washington, Q. Fu,
557 D. R. Sikka, and M. Wild (2005), Atmospheric brown clouds: Impacts on South Asian
558 climate and hydrological cycle, *Proceedings of the National Academy of Sciences of the*
559 *United States of America*, *102*(15), 5326–5333, doi:10.1073/pnas.0500656102.

560 Roberts, G. C., M. O. Andreae, W. Maenhaut, and M. T. Fernandez-Jimenez (2001),
561 Composition and sources of aerosol in a central African rain forest during the dry season, *J.*
562 *Geophys. Res*, *106*(D13), 14423–14434, doi:10.1029/2000JD900774.

563 Rosenfeld, D. et al. (2014), Global observations of aerosol-cloud-precipitation-climate
564 interactions, *Rev. Geophys.*, *52*(4), 750–808, doi:10.1175/1520-
565 0493(1994)122<1837:DCCSIT>2.0.CO;2.

566 Saleh, R. et al. (2014), Brownness of organics in aerosols from biomass burning linked to their
567 black carbon content, *Nature Geoscience*, *7*(9), 647–650, doi:10.5194/acp-11-7669-2011.

568 Satheesh, S. K., and V. Ramanathan (2000), Large differences in tropical aerosol forcing at the
569 top of the atmosphere and Earth's surface, *Nature*, *405*(6782), 60–63.

570 Sato, Y., D. Goto, T. Michibata, K. Suzuki, T. Takemura, H. Tomita, and T. Nakajima (2018),
571 Aerosol effects on cloud water amounts were successfully simulated by a global cloud-
572 system resolving model, *Nat Commun*, *9*(1), 1227, doi:10.1256/qj.03.187.

573 Science, N. M., 2011 (2011), Aerosol indirect effect on biogeochemical cycles and climate,
574 *science.sciencemag.org*, *334*, doi:10.1126/science.1207374.

575 Seinfeld, J. H. et al. (2016), Improving our fundamental understanding of the role of
576 aerosol–cloud interactions in the climate system, *Proceedings of the National Academy of*
577 *Sciences of the United States of America*, *113*(21), 5781–5790,
578 doi:10.1073/pnas.1514043113.

579 Streets, D. G., Y. Wu, and M. Chin (2006), Two-decadal aerosol trends as a likely explanation of
580 the global dimming/brightening transition, *Geophys. Res. Lett*, *33*(15), L17802–25,
581 doi:10.1029/2006GL026471.

582 Streets, D., Zhang, Q., Wang, L., He, K., Hao, J., Wu, Y., Tang, Y., and Carmichael, G.:
583 Revisiting China's CO emissions after the Transport and Chemical Evolution over the
584 Pacific (TRACE-P) mission: Synthesis of inventories, atmospheric modeling, and
585 observations, J. Geophys. Res.-Atmos., 111, D14306, doi:10.1029/2006JD007118,
586 2006.T.C. Bond et al. Historical emissions of black and organic carbon aerosol from energy-
587 related combustion, 1850-2000, Global Biogeochemical Cycles, 21 GB2018, doi:
588 10.1029/2006GB002840, 2007

589 Van Damme, M., L. Clarisse, S. Whitburn, J. Hadji-Lazaro, D. Hurtmans, C. Clerbaux, and P.-F.
590 X. O. Coheur (2018), Industrial and agricultural ammonia point sources exposed, *Nature*, 1–
591 12, doi:10.1038/s41586-018-0747-1.

592 van der Werf, G. R. et al. (2017), Global fire emissions estimates during 1997–2016, *Earth Syst.*
593 *Sci. Data*, *9*(2), 697–720, doi:10.5194/acp-9-5785-2009.

594 van der Werf, G. R., Randerson, J. T., Giglio, L., van Leeuwen, T. T., Chen, Y., Rogers, B. M.,
595 Mu, M., van Marle, M. J. E., Morton, D. C., Collatz, G. J., Yokelson, R. J., and Kasibhatla,

P. S. (2017). Global fire emissions estimated during 1997–2016. Earth Syst. Sci. Data, 9(2):697–720.

van der Werf, G. R., J. T. Randerson, L. Giglio, G. J. Collatz, M. Mu, P. S. Kasibhatla, D. C. Morton, R. S. Defries, Y. Jin, and T. T. van Leeuwen (2010), Global fire emissions and the contribution of deforestation, savanna, forest, agricultural, and peat fires (1997–2009), *Atmospheric Chemistry and Physics*, *10*(23), 11707–11735, doi:10.5194/acp-10-11707-2010.

van Donkelaar, A., R. V. Martin, M. Brauer, and B. L. Boys (2015), Use of Satellite Observations for Long-Term Exposure Assessment of Global Concentrations of Fine Particulate Matter, *Environmental Health Perspectives*, *123*(2), 135–143, doi:10.1289/ehp.1408646.

Vestreng, V. and Klein, H.: Emission data reported to UNECE/EMEP, Quality assurance and trend analysis Presentation of WebDab,Norwegian Meteorological Institute ,Oslo, Norway, MSC-W Status Report, 2002.

Warner, J. X., R. R. Dickerson, Z. Wei, L. L. Strow, Y. Wang, and Q. Liang (2017), Increased atmospheric ammonia over the world's major agricultural areas detected from space, *Geophys. Res. Lett*, *44*(6), 2875–2884, doi:10.1002/2016GL072305.

Worden, H. M., A. A. Bloom, J. R. Worden, Z. Jiang, E. A. Marais, T. Stavrakou, B. Gaubert, and F. Lacey (2019), New constraints on biogenic emissions using satellite-based estimates of carbon monoxide fluxes, *Atmospheric Chemistry and Physics*, *19*(21), 13569–13579, doi:10.5194/acp-19-13569-2019.

Worden, J. et al. (2009), Observed vertical distribution of tropospheric ozone during the Asian summertime monsoon, *J. Geophys. Res*, *114*(D13), D13304, doi:10.1029/2008JD010560.

Worden, J. R., A. A. Bloom, S. Pandey, Z. Jiang, H. M. Worden, T. W. Walker, S. Houweling, and T. Röckmann (2017), Reduced biomass burning emissions reconcile conflicting estimates of the post-2006 atmospheric methane budget, *Nat Commun*, 1–11, doi:10.1038/s41467-017-02246-0.

623 Yin, Y., F. Chevallier, P. Ciais, G. Broquet, A. Fortems-Cheiney, I. Pison, and M. Saunois
624 (2015), Decadal trends in global CO emissions as seen by MOPITT, *Atmospheric Chemistry*
625 *and Physics*, *15*(23), 13433–13451, doi:10.5194/acp-15-13433-2015.

626 Zhao, B., J. H. Jiang, Y. Gu, D. Diner, J. R. Worden, K. N. Liou, S. HH, X. J, M. J. Garay, and
627 L. Huang (2017), Decadal-scale trends in regional aerosol particle properties and their
628 linkage to emission changes, *Environ. Res. Lett.*, doi:10.1088/1748-9326.

629